MISSOURI S&T

Missouri University of Science and Technology

Scholars' Mine

International Conferences on Recent Advances in Geotechnical Earthquake Engineering and Soil Dynamics

2010 - Fifth International Conference on Recent Advances in Geotechnical Earthquake Engineering and Soil Dynamics

26 May 2010, 4:45 pm - 6:45 pm

Seismic Performance Assessment in Dense Urban Environments: Evaluation of Nonlinear Building-Foundation Systems Using Centrifuge Tests

ZhiQiang Chen
University of California at San Diego, La Jolla, CA

Tara C. Hutchinson
University of California at San Diego, La Jolla, CA

Nicholas W. Trombetta
University of California at San Diego, La Jolla, CA

Henry B. Mason
University of California at Berkeley, Berkeley, CA

Jonathan D. Bray
University of California at Berkeley, Berkeley, CA

Follow this and additional works at: https://scholarsmine.mst.edu/icrageesd

Part of the Geotechnical Engineering Commons

See next page for additional authors

Author

ZhiQiang Chen, Tara C. Hutchinson, Nicholas W. Trombetta, Henry B. Mason, Jonathan D. Bray, Katherine C. Jones, Chandrakanth Bolisetti, Andrew S. Whittaker, Benjamin Y. Choy, Bruce L. Kutter, Gregg L. Fiegel, Jack Montgomery, Roshani J. Patel, and Robert D. Reitherman

SEISMIC PERFORMANCE ASSESSMENT IN DENSE URBAN ENVIRONMENTS: EVALUATION OF NONLINEAR BUILDING-FOUNDATION SYSTEMS USING CENTRIFUGE TESTS

ZhiQiang Chen, Tara C. Hutchinson and Nicholas W. Trombetta
University of California at San Diego
La Jolla, CA-USA 92093

Henry B. Mason, Jonathan D. Bray and Katherine C. Jones
University of California at Berkeley
Berkeley, CA-USA 94720

Chandrakanth Bolisetti and Andrew S. Whittaker
University of Buffalo
Buffalo, NY-USA 14260

Benjamin Y. Choy and Bruce L. Kutter
University of California at Davis
Davis, CA-USA 95616

Gregg L. Fiegel, Jack Montgomery and Roshani J. Patel
Cal Poly – San Luis Obispo
San Luis Obispo, CA-USA 93407

Robert D. Reitherman
CUREE
Richmond, CA-USA 94804

ABSTRACT

In dense urban areas, buildings are generally constructed in clusters, forming city blocks. New buildings are designed assuming their response is independent of adjacent buildings, which ignores potentially important structure-soil-structure-interaction (SSSI) effects. Although a few studies have revealed the significance of SSSI effects, validated simulation and design tools do not exist. In this paper, we present the results from the first in a series of centrifuge tests intended to investigate SSSI effects. Results herein are focused on the design and measured response of two model building-foundation systems placed on dense dry Nevada sand and tested at 55-g. The two models represent prototypical nine-story and three-story special moment resisting frame buildings, with the former structure supported by a three-level basement-mat and the later on isolated spread footings. Nonlinear response-history simulations are performed to aid in the design of the models, with particular attention to reproducing prototype building periods and nonlinear characteristics. Yielding of the model buildings is achieved using custom-designed fuses placed strategically throughout the super-structures. At present, the two models are placed as far apart as possible to characterize soil-structure interaction on individual buildings; subsequent experiments will move the structures in near proximity, allowing direct experimental assessment of structure-soil-structure-interaction.

INTRODUCTION

Soil-foundation-structure-interaction (SFSI) has been studied since the 1960's. Field data indicate that for buildings supported on shallow foundations, the building period including the effects of SFSI can be up to 1.5 times that of the fixed-base system, the foundation damping due to soil radiation and hysteresis can be between 10 and 15%, and the spectral ratio of the foundation input motion to the free field motion may be as low as 0.5. SFSI effects result from complicated material and geometric nonlinearities, which may include soil inelasticity, gapping between the foundation and the soil, slippage at the soil-foundation interface, base uplifting and rocking, and loss of soil strength (e.g., due to excessive pore water pressures). In addition, as waves scatter from the foundation, radiation damping is developed, which strongly depends on the aforementioned nonlinearities. These SFSI mechanisms and effects have been investigated using a variety of analytical and numerical techniques. Early efforts included development of impedance functions using elastic-half space theory (e.g., Luco, 1969; Trifunac, 1972; Veletsos and Meek, 1974; Bielak, 1975). In the following section, design-oriented procedures and simplified simulation methods to account for SFSI are discussed.

Design and Simulation to Account for SFSI

SFSI effects have been traditionally ignored in design practice. Besides the desire to simplify the analysis, a primary argument for doing so by design engineers is that period lengthening and augmented system damping when SFSI is accounted for usually results in reduced spectral response ordinates, leading to a conservative design. In addition, from an energy-absorption point of view, engineers have realized that rocking of structures on shallow foundations can effectively dissipate earthquake-induced energy (e.g., Housner, 1963).

This simplification, however, is only valid for certain classes of building-foundation systems; namely light, flexible structures on stiff soil. Detrimental SFSI effects have been reported by many researchers (e.g., Stewart et al., 1999; Mylonakis and Gazetas, 2000). Effects include, for example,

(i) resonance during low-frequency dominated ground shaking due to lengthened system periods with increased seismic demands, (ii) increased structural drift due to foundation rocking and sliding, which may lead to unconservative estimates of displacement, serviceability issues and building pounding, and (iii) over-loaded soil and foundation deformations (particularly settlement) may further degrade performance and damage the superstructure. There is increasing consensus that SFSI effects, beneficial or detrimental, should be considered when designing new or retrofitting existing buildings in the context of performance-based earthquake engineering (PBEE) (e.g., Stewart et al. 1999; Pecker and Pender 2000; Martin and Lam 2000; Pitilakis et al. 2004, Gajan et al. 2009).

Recent code-based procedures have addressed many aspects of considering SFSI in structural design. ASCE-41 (ASCE, 2006) and related design documents address flexible foundation effects by considering the stiffness of the foundation and compliance of soil. These procedures do not include the possible response-reduction factors due to foundation-soil kinematic interaction and foundation-soil damping. FEMA 440 (FEMA, 2005) recommends simplified procedures for characterizing the foundation input motion (FIM) and system damping. For example, the FIM can be computed by applying a low-pass filter in the frequency domain. This computation is intended to account for slab-averaging and embedment-induced kinematic effects on the free-field motion (FFM). However, studies show that using code-based procedures that do not account for some SFSI effects such as foundation uplifting can result in un-conservative response predictions. For example, Harden et al. (2006) indicates that the nonlinearity introduced by uplifting of and yielding below shallow foundations can increase displacements resulting in overstress to some structural components.

Recently, numerical methods to account for nonlinear SFSI have received substantial attention. Two predominant types of methods emerge, namely lumped macro-element method and distributed spring-based element method (e.g., Gajan et al., 2009). Macro-elements lump the foundation-soil response at single elements interfacing between the structure and the supporting foundation (e.g., Cremer et al., 2001; Gajan and Kutter, 2009). In contrast, spring-based elements are discretely distributed combinations of springs, gap elements, and dashpots (e.g., Gerolymos and Gazetas, 2006; Raychowdhury and Hutchinson, 2009). Limitations exist with either method, with the former lacking the provision to provide distributed response data for the foundation (e.g. sectional forces along a strip footing), and the latter typically formulated absent coupling between the various directions of response.

SSSI Effects in a City-Block

In dense urban areas, buildings are generally constructed in clusters, forming city blocks. Therefore, neighboring building-foundation systems are not physically independent, and mechanical interaction occurs between them during a seismic event, resulting in complex structure-soil-structure-interaction

(SSSI) effects. Perhaps the earliest analytical modeling effort related to SSSI effects is that presented by Luco and Contesse (1973). In this work, the authors derive an analytical half-space solution for the problem of two adjacent shear wall buildings subjected to anti-plane vertically-incident SH waves. Anti-plane in this context means that the motion of the soil particles is normal to the plane of the building array. Wong and Trifunac (1975) extend this problem to multiple buildings subjected to arbitrarily incident SH waves. In addition to the significant modification of the ground response due to the presence of an array of buildings, both papers confirm that SSSI is most prominent if the structure of interest is smaller and lighter than its neighboring structures. Most recent studies using similar analytical models (i.e. a 2D building array subject to anti-plane SH waves) have been used to explain the seismic recordings in a densely built urban environment during the 1995 Mexico City earthquake (e.g. Kham and Semblat, 2006; Grobya and Wirgin, 2008; Ghergu and Ionescu, 2009). Numerical modeling of building-foundation systems coupled to the soil to understand SSSI effects has seen less attention in the literature. In an early study by Lee and Wesley (1973) the authors simulate the 3D response of three adjacent nuclear structures. They conclude that dynamic response of structures can be significantly modified due to coupling through the soil. Recent work by Bielak et al. (2005), include spatially distributed buildings resting on a detailed finite element soil model. Their model is able to evaluate the spatial distribution of structural damage during a seismic event; however, building proximity is not considered.

Although the aforementioned, limited number of studies have revealed the significance of SSSI effects in modifying structural and ground response, validated simulation and design tools do not exist. To advance performance-based earthquake engineering (PBEE), the US National Science Foundation funded a research project that includes a series of physical model experiments using the NEES@UCDavis geotechnical centrifuge. The physical models are designed with realistic material and system-level structural nonlinearities. Nonlinear structural response is sought in these models to characterize the expected response of code-compliant buildings subjected to earthquake shaking. Data generated from these experiments will be used to validate numerical models and support development of design procedures for the explicit consideration of SFSI and SSSI effects.

Scope and Organization

In this paper, we present the design, experimental program, and results from the first series of tests (denoted as Test-1) of this project, with a focus on the building-foundation systems. A companion paper focuses on the ground motion and soil aspects of the test program (Mason et al., 2010). For Test-1, two buildings are designed with behavior intended to reproduce that of prototypical nine-story and three-story special moment resisting frame buildings, with the former supported by a three-level basement-mat and the latter on isolated spread footings. Nonlinear response history

simulations are performed to aid in the design of the models with particular attention given to capturing building fundamental periods and nonlinear characteristics. Yielding of the centrifuge models is achieved by custom-designed fuses placed strategically throughout the models. The models are subjected to 17 earthquake motions of increasing intensity in a 55-g environment. The motion selection and site response characteristics from Test-1 are presented in Mason *et al*. (2010). For Test-1 the models are placed as far apart as possible in the centrifuge, that is, isolated from each other. In subsequent test series the models will be sited close to one another, replicating a dense urban region, which will facilitate a direct experimental assessment of structure-soil-structure-interaction (SSSI). The results of Test-1 serve as a benchmark for all subsequent experiments.

In the following sections, we first present the design of the physical models based on selected prototype buildings. Predicted fixed-base and flexible-base properties are summarized. The experimental program for Test-1 is described in terms of the construction, instrumentation and testing protocol. Measured results are presented, with foci on (i) identification of modal frequencies of both model structures following each shaking event, and (ii) detailed global and local structural response analysis considering SFSI. Prototype units are used unless otherwise noted. A summary of scaling laws applied to this test can be found in Mason *et al*. (2010).

DESIGN OF TWO BUILDING-FOUNDATION MODELS

Prototype Building Parameter Space

Design parameters associated with those found in practice are sought to guide the design of the physical models. Extending the SAC work, Ganuza (2006) developed a broad range of building types and configurations and associated numerical models (Figure 1) for modern code-compliant building construction in Los Angeles. Through consultation with practicing engineers, it is felt that this type of urban environment consists primarily of low- to mid-rise buildings. Common types of lateral load resisting systems are eccentrically braced frames, special moment resisting frames, and reinforced concrete walls. The fundamental periods of these systems are estimated to range from about 0.2 to 2.5 seconds, with yield strength ratios ranging from 0.15 to 0.55 (Figure 1).

Of the range of characteristics within the prototype building space, for Test-1 the two selected prototype buildings are both SMRF buildings, one three stories in height and the other nine stories in height. The prototype properties of these buildings are listed in Table 1 and are used as the target values to design the physical models. In this table, T_n is the nth -- modal period, V_y/W is the ratio of yield strength to reactive weight, and γ_y is the drift ratio at yield of the frame.
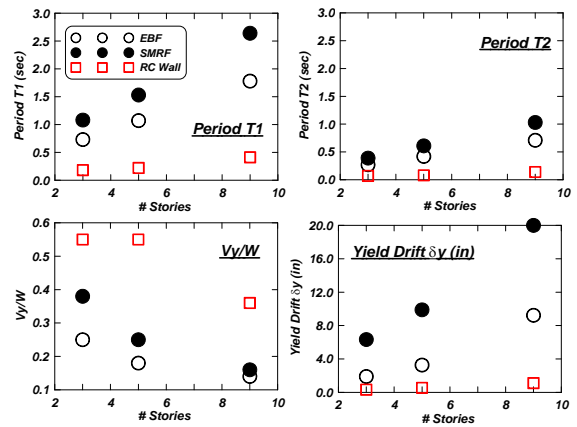

Fig. 1. Parameter space used to select the prototype building properties (data from Ganuza, 2006).

Table 1: Target structural properties of the prototype buildings (termed *lam123* and *lam19* in Ganuza, 2006).

Reference	Structure Type	T_n(sec)	V_y/W	γ_y (%)
lam19	SMRF, 9-story	2.6, 0.8, 0.5	0.2	1.4
lam123	SMRF, 3-story	1.1	0.3	1.2

Model Building Properties

The prototype buildings were to be constructed at a centrifuge scale of N = 55. However, rather than geometrically scaling the buildings directly by N, a single story model building is used to capture the key features of the 3-story prototype building, while a 3-story model building is used to capture the key features of the 9-story building (Table 1). In the model design, we sought to reproduce the first 3 translational modes of response for the 9-story building and the first translational mode for the 3-story building. Capturing these modes in the model buildings is sufficient, as they contribute more than 95% of the total reactive mass of the prototype buildings.

Obtaining available material for the model construction partially guides member selection. In this case, steel square tubing (1/2" x 1/2" x 1/16") is selected to construct the beams and columns. To introduce structural nonlinearity and to adjust the stiffness of the model structures, sections at the beam-column ends and column bases are intentionally reduced using strategically placed fuses. Three fuse sections are designed (Figure 2). The configuration of the two model buildings, denoted as MS1F_SF80 and MS3F_B, are summarized in Tables 2 and 3. Two-dimensional schematic plots of these models are shown in Figure 3. Photographs of the building models placed in the centrifuge container are presented in Figure 4.
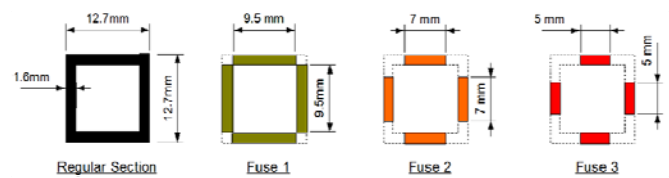

Fig. 2. Member cross sections used throughout the building models (units: model scale).

Table 2: Configuration of models – superstructure
(units: model scale)

Name.	Plan View L x B (mm)	Elevation View L x ({Hn}) (mm)	Floor Mass (kg)
MS3F_B	200.0 x 200.0	200.0 x (231.8; 200.0; 200.0)	3.97 (M2), 3.12 (M1)
MS1F_SF80	181.0 x 200.0	181 x 231.8	4.11 (M3)

Table 3: Configuration of models – foundations
(units: model scale)

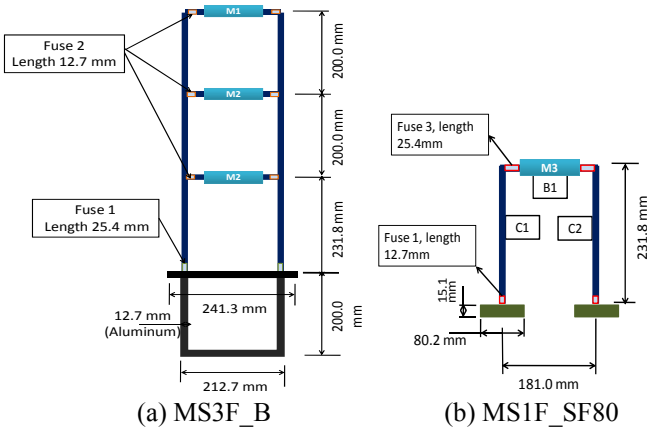| Name	Foundation Types	Foundation L_f x B_f x H_f (mm)	D_f (mm)	Foundation Mass (kg)
MS3F_B	Basement on mat	200.0 x 200.0 x 200.0 (t_w=12.7mm)	200.0	8.50
MS1F_SF80	Isolated spread footings	79.4 x 79.4 x 15.9	21.0	3.14

Fig. 3. Schematic 2D illustration of model building-foundation structures. (units: model scale).
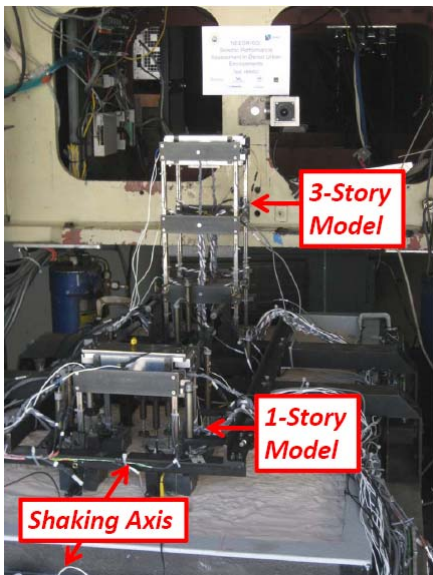

Fig. 4. Photograph of building-foundation models in Test-1.

To understand the behavior of the models, OpenSees (Mazzoni *et al.*, 2009) based numerical models were created. The *BeamwithHinges* element is used to model the structural beams and columns. The inertial interaction of the building-foundations with the soil is modeled using the concept of beam-on-nonlinear-Winkler-foundations (BNWF) (Figure 5), wherein the soil is replaced by a series of Py, Qz and Tz springs implemented in OpenSees (Boulanger, 2000). The discretization scheme and parameter selection protocols for the BNWF footing model follows the work of Raychowdhury and Hutchinson (2009).
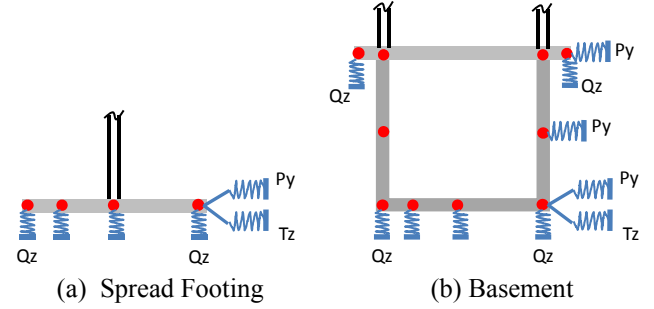

Fig. 5. BNWF discretization schemes for the spread footings and the basement foundation using Py, Qz and Tz inelastic springs (9 Qz, 1 Py and 1 Tz are used in (a); 15 Qz, 3 Py and 1 Tz are used in (b)).

With the above configuration, both fixed- and flexible-base numerical simulations are conducted. Table 4 documents the fixed-base periods and the realized target parameters by conducting nonlinear static (pushover). Impulse (tap) tests were conducted to identify the fixed-base modal periods of the constructed models. Results in Table 4 indicate that these agree well with the OpenSees predictions. Table 5 provides the eigenvalue analysis results considering foundation flexibility (to differentiate, the subscript *ssi* is adopted). Reasonable agreement is observed between the numerical model and the estimates using the method of Veletsos and Meek (1974).

Table 4: Achieved prototype properties of the buildings, based on OpenSees simulation and identified from tap tests

No.	OpenSees			Tap Test
	T_{fix}^{S} (sec)	γ_y^{S} (%)	$(V_y/W)^S$	T_{fix}^{T} (sec)
MS3F_B	2.36, 0.71, 0.39	1.66	0.21	2.50, 0.69, 0.35
MS1F_SF80	1.06	1.72	0.59	1.10

Table 5: Comparison of OpenSees simulation periods with prediction based on procedure of Veletsos and Meek (1974)

No.	OpenSees		Veletsos and Meek, 1974
	T_{ssi}^{S} (sec)	T_{ssi}^{S}/T_{fix}^{S}	$T_1^{VM}/T_{fix,1}^{S}$
MS3F_B	3.31, 0.73, 0.40	1.40, 1.03, 1.03	1.2
MS1F_SF80	1.60	1.51	1.6

Note: $G = 0.1 G_{max}$, where $G_{max} = 80$ *GPa*, is used in computing the Gazetas stiffnesses (FEMA, 2000).

TEST-1 DESCRIPTION

The overarching goal of Test-1 is to characterize the performance of two physical models of building-foundation systems acting independently of each other to a suite of ground motions designed to cause increasing structural damage and nonlinearity. Herein, we describe Test-1 in terms of the special considerations given to test design due to the use an earthquake shaking protocol with progressively increasing intensities, the instrumentation required to reach the test goal, and a critique of the instrumentation performance within the harsh environment of a high g-level spinning centrifuge.

Progressive Shaking Scenario

It was estimated to take approximately 1 hour to spin-up, reach the target revolutions per minute (RPM), and spin-down for each centrifuge experiment. For this reason, it was determined that multiple ground motions would be applied to the model during each spin. Therefore, special precautions were needed to ensure the foundation-structure system and the instrumentation performance remained reasonable during progressive development of structural damage. These considerations include: special care in the selection of the order of applied ground motions; structural details to allow for in-situ retrofit between spins; and the need for rapid but informative data processing between each motion.

Preliminary nonlinear response-history simulations, performed using OpenSees, allowed us to determine the intensity of ground motions for the building-foundation systems. Maximum predicted curvature ductility demands (μ_ϕ) and number of inelastic cycles in the hinges of two models, as well as spectral accelerations guided the preliminary ranking of the ground motions from least to most damaging. Table 6 documents these results.

Table 6. Spectral accelerations and predicted damage quantities for individual motions

Motion ID	Sa(T1$_{ssi}$) (g)		Max μ_ϕ	No. of Inelastic Cycles
	MS1F_SF80	MS3F_B		
JOS_L	0.22	0.05	0.76	0
TCU	0.15	0.02	0.62	0
SCS_L	0.33	0.06	1.29	4
RRS	0.35	0.10	1.31	2
LCN	0.39	0.17	2.47	4
PTS	0.32	0.16	2.84	9
WVC	0.37	0.22	3.42	7
SCS_H	0.71	0.14	3.83	6
JOS_H	0.54	0.11	2.67	5
WPI	0.65	0.16	3.34	5
PRI	0.57	0.20	3.33	12

Once the ranking was established, the preliminary ground motion order was input into OpenSees as a progressive shaking scenario where the damaged structure from the previous motion served as the starting point for the next motion. Due to the predicted relatively high plastic demands in the later motions, the beam-column connections were designed to accommodate a straightforward retrofitting of the fuses in-situ. This simple, pragmatic step allowed for replacement of damaged components between spins. In addition, by resetting the superstructures to their original state through retrofit of yielding components, it was possible to impose large motions without fear of collapse due to progressive damage. The final ordered ground motions used in Test-1 is provided in Mason *et al* (2010) .

Building-Foundation Model Instrumentation

The building-foundation systems were instrumented with 157 transducers: 22 linear displacement potentiometers, 39 uniaxial accelerometers, and 96 strain gages. Fifty transducers were used to measure the response of the soil; see Mason *et al*. (2010) for details.

The NEES Equipment Site at UC Davis (UCD) was able to provide two types of instrumentation for use in characterizing the structures: uniaxial accelerometers with measurement ranges of ±50g, ±100g, and ±200g; and linear displacement pots with measurement ranges from ±0.5in to ±3in. Strain gages were used to capture localized strains and enable resolution of forces at important locations throughout the models. Three types of strain gages were used: standard elongation uniaxial gages, which measure up to 3000 $\mu\varepsilon$; standard elongation triaxial strain rosettes, which measure up to 3000 µε along three separate axes spaced at 45°; and high elongation uniaxial gages, which measure up to 15000 $\mu\varepsilon$.

The placement of accelerometers throughout both MS1F_SF80 and MS3F_B allowed for measurement of all relevant structural and foundation accelerations during each shaking event. Three accelerometers placed at the center of each floor's mass captured floor level accelerations along the direction of shaking (North-South), orthogonal to the direction of shaking (East-West), and vertically. A fourth accelerometer, placed facing North-South near the edge of the floor mass, provided, along with the accelerometer through the center of mass, a measurement of the torsional motion. Figure 6 shows the location of the superstructure accelerometers and displacement potentiometer on a typical floor.

Accelerometers were placed on the foundations to allow for determination of the input motions to the structures and comparison of them to the soil surface level accelerations. Three accelerometers, one horizontal and two vertical, placed on the spread footings supporting MS1F_SF80 captured horizontal, vertical, and rocking accelerations of each individual footing. Nine accelerometers were placed on the basement-mat foundation to characterize its six degrees of freedom. Figure 7 presents the layout for foundation level accelerometers on model MS3F_B.
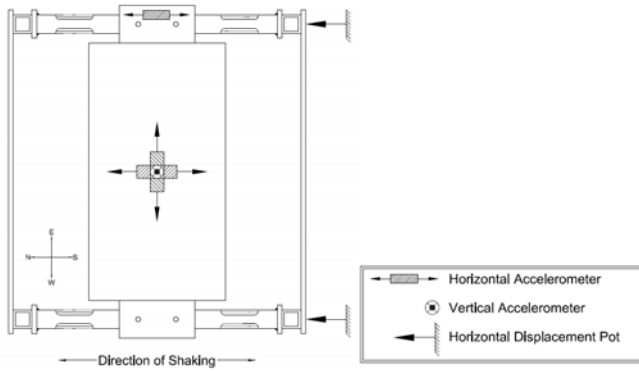
Fig. 6. Location of Acceleration and Displacement Measurements for a Typical Floor
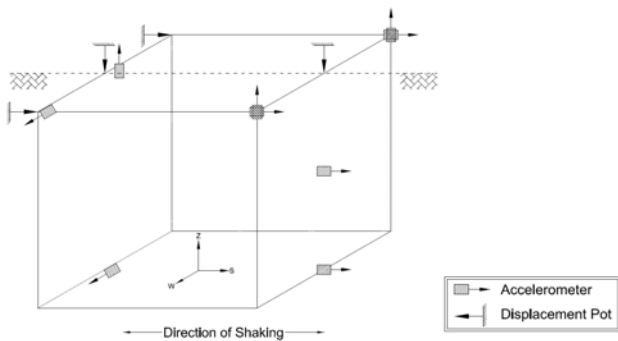

Fig. 7 Accelerometers and Linear Displacement Potentiometers on the Basement-Mat Foundation of MS3F_B.

Linear displacement pots were placed throughout both building-foundation systems to measure displacements. Two displacement measurements, parallel to the direction of shaking, taken at each floor level provided measurements of both dynamic and permanent story drifts. A single horizontal potentiometer on the footings supporting MS1F_SF80 provided dynamic and permanent sliding data. Two vertical pots on each F3 and F4 provided transient and residual data for settlement and rocking. Two horizontal potentiometers placed at the soil-surface level measured sliding and torsional motion of the basement-mat foundation supporting MS3F_B. In addition, two vertical pots provided measurements of foundation settlement and rocking (Figure 7). Laterally spanning racks were used to provide reference points for the displacement measurements.

Strain gages were placed throughout the models to enable assessment of structural damage and resolution of sectional forces. A high elongation strain gage placed on the top and bottom flange of the fuses captured nonlinear post-yield strains in these locations. These strains lead to the calculation of section curvature and bending moment using information from calibration tests conducted under pure bending. A pair of standard elongation strain gages placed below the beam-column connection at each floor provided curvature and moment data in these locations. Standard elongation gages were adequate in these locations because the structural details allowed yielding at the designed hinge locations only. Finally,

strain rosettes placed at the mid-floor height of each column are used to compute shear strain and shear force in each column. Figure 8 shows the placement of strain gages throughout MS1F_SF80 (the placement throughout MS3F_B is similar).
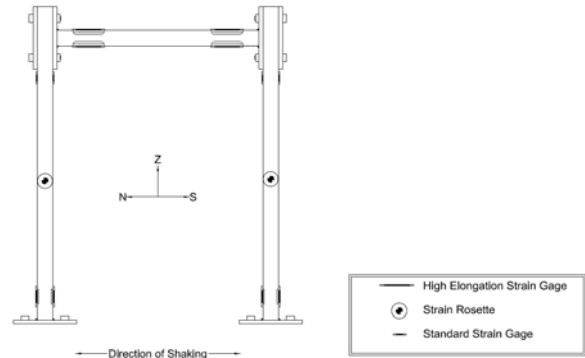

Fig. 8. Location of strain measurements on MS1F_SF80

Instrumentation Performance

The centrifuge environment is harsh on instrumentation and as a result, special attention must be provided to issues not typically observed when testing in the 1-g environment. In this case for example, with over 200 sensors, the effects of instruments and their associated cabling (particularly their weight) and location are important. Two key issues affected the performance of instrumentation during Test-1: the design and construction of reference frames for displacement measurements; and the use of 96 quarter-bridge strain gages between the two structures.

To measure reliably transient displacements, the reference frames in the centrifuge box should be very stiff. Complicating the design of the reference frame for Test-1 was not only the height of MS3F_B above the soil-surface, but also the spacing between the structures. Ultimately it was observed that the reference frames deflected significantly under increased gravity. Observations from the high-speed video revealed that pots also lost contact with the structure during severe shaking events. As a result, dynamic displacement measurements from many of the potentiometers do not provide reliable data. Inspection of the frames between spins revealed that all frame displacements experienced during earthquake motions were elastic therefore permanent displacement measurements from these potentiometers are valid. Given the poor performance of the reference frames used in Test-1, the racks will be stiffened substantially for Test-2.

Strain gage performance needed to be assessed in the context of: (i) their usability under increased gravitational load and (ii) the complexity of their connection to the data acquisition system. Careful strain relief on the gage-lead wire connections under increased gravitational loads was necessary, and was achieved through a variety of methods. The complexity of using only quarter-bridge measurements also led to issues with

strain gage performance. Prior to Test-1, the UCD Centrifuge was only capable of handling 32 quarter-bridge strain gages, but the instrumentation planned called for 96 gages. A series of modifications to the data acquisition system, requiring more than 2000 new electrical connections, allowed for the exclusive use of quarter bridge measurements. Ultimately the number of surviving strain gages after each spin was greater than expected and they have provided an extremely robust local damage data set.

RESPONSE OF THE MODEL BUILDING-FOUNDATION SYSTEMS: CASE STUDY OF A HIGH INTENSITY NEAR FAULT (HI-NF) MOTION (LCN)

In this section, we present results of the analysis of the building-foundation systems for one of the earthquake ground motions. A subsequent section will summarize the results of analyses for all motions. The selected motion is 'LCN', the 260 degree component measured at Lucerne, during the 1992 Landers earthquake. This motion is classified as 'near-fault' (NF) and 'higher-intensity' (HI), with recorded peak ground acceleration and ground velocity of 0.26g and 44 cm/sec at surface, respectively (Mason *et al.*, 2010). Analysis of measurements from this motion involves first studying the global behavior of the model via peak accelerations and displacements, and subsequent evaluation of the local behavior of the fuses.

Global Structural Response

Figure 9(a) presents the acceleration response of the model, as propagated from the input, through the soil column, and to the roof of the 1-story model structure MS1F_SF80. Note that the acceleration record measured at the surface of the soil is treated as 'free-field' motion (FFM). In Figure 9(b), the measured motions are then used to compute the spectral acceleration values $Sa(T1)$ with $T1$ ranging from 0.1 to 10 seconds. Similar to Figure 9(a), the spectral plots are arranged following the elevation of the sensors. Noted that in generating these elastic spectral acceleration plots, 5% system damping is assumed.

One may observe first that the base input is amplified through the soil column; second, although the frequency content of the response of the footing and the FFM at the surface seem similar, which is confirmed by their spectral plots in Fig. 9(b), the peak soil acceleration was not captured by the footing. This de-amplification may be attributed to minor kinematic interaction or isolation effects. The model structure amplified the zero-period FFM at the soil surface (from 0.38 g to 0.43 g), with an un-correlated acceleration amplification factor of approximately 1.13. The peak acceleration responses occur at about the same time. However, in the spectral domain, one may see that the occurrence of the peak spectral coordinates shifts from $T1 = 0.6$ sec to $T1 = 1.2$ sec between the roof response and the FFM at the soil-surface.
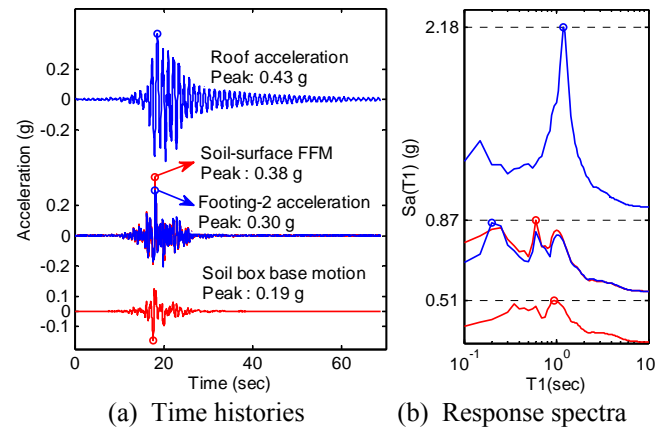

(a) Time histories   (b) Response spectra

Fig. 9. Accelerations resulting from motion LCN of model MS1F_SF80: (a) time-series plots from soil, footing, to the roof; (b) elastic acceleration response spectral plots.

Figure 10 offers similar plots as those in Figure 9 for the model MS3F_B. In addition to the surface level FFM, the FFM aligned with the bottom of the basement is shown in Figure 10. Consistent with measurements presented previously for the 1-story model, the soil column amplifies the input motion at the surface. However, the motion amplifies and then de-amplifies as it propagates through the super-structure. De-amplification is particularly noted on the second floor. This can be attributed to the contribution of the second mode of response of the building. In contrast to observations in Figure 9(a), the peaks of the acceleration response at the floors occur at about the same time. They do however shift from the instance in time when peaks are observed in the soil. In the spectral plots, the peak $Sa(T1)$'s of the response signals occur at $T1 = 0.75$ sec. Recall that the second mode of MS3F_B is 0.73 sec (note that in computing $Sa(T1)$, the period interval is 0.05 sec; hence the exact $T1$ at which $Sa(T1)$ has peak may vary but be close to 0.75 sec). At the basement levels, both the foundation response and the two soil FFM inputs have a peak $Sa(T1)$ at 0.6 sec, whereas the $Sa(T1)$ for the soil box base motion peaks at $T1 = 0.95$ sec.

Displacement demands in terms of total roof displacement and total drift ratio of the models due to motion LCN are reported in Figure 11. These two records are initialized to zero, removing any permanent deformation resulting from prior tests. In addition, the deformations in these plots include the contribution of the foundation sliding and rocking. A residual displacement is observed for model MS1FS but not for model MS3FB. The total peak drift ratio was 0.86 and 1.81% for models MS3F_B and MS1F_S, respectively. Noting that minimal foundation movement was observed for MS3F_B, this total peak drift ratio is well below the yield drift ratio predicted for the structure, indicating that plastic structural deformations did not develop during this motion. In contrast, MS1F_S likely observed plastic deformations (either soil or structural, this plot cannot reveal this information), due to its large total maximum drift ratio (refer to Table 4).
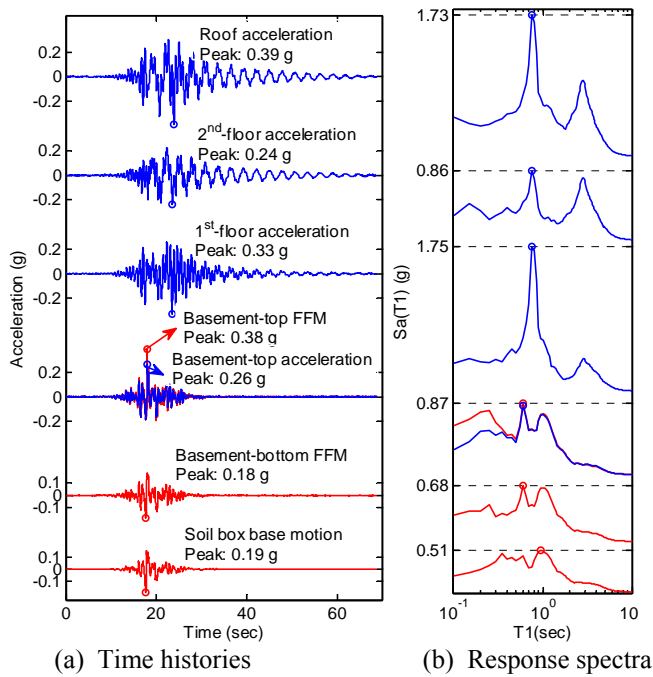
Fig. 10. Accelerations resulting from motion LCN – model MS3F_B: (a) measured acceleration records from soil, basement, to the roof; (b) elastic acceleration response spectral plots.
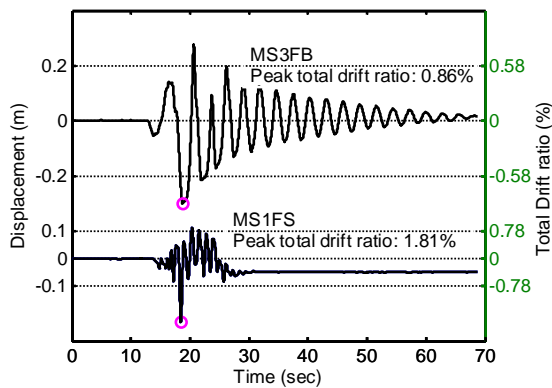

Fig. 11 Total roof displacements and drift ratios of MS1F_SF80 and MS3F_B subjected to motion LCN.

Fuse Behavior

The time-series plots in Figure 12 show the strain histories measured at the top and bottom flanges of the northwestern-most hinges in both MS1F_SF80 and MS3F_B during the first six motions. This data shows that plastic strain is first observed in the MS1F_SF80 model fuses as early as the third earthquake motion, RRS. Motion RRS is classified as a higher intensity near fault (HI-NF) motion, with a peak input acceleration and input velocity of 0.39 g and 34 cm/sec, respectively (Mason *et al.*, 2010). Note that yielding is observed even though the measured strains did not reach the material yield strain of 2200 $\mu\varepsilon$. Yield strain is likely not measured in this case as the plastic strains occurred at a location other than the strain gages. In this case, post-spin

down physical observation of the model indicated that yielding regions were concentrated near the ends of the hinges (Figure 13). The strain gages span the entire length of the fuse flanges and are therefore an average of both the strains experienced by the yielded portions and elastic portions of the hinges. Additionally, the hinges were instrumented assuming a bending-dominated failure mode over the length of the hinges, while yielding was observed to occur at the two ends of the hinges during the shaking events, showing a shear-like failure shape. This unexpected failure mode for the Northwestern fuse can be observed from the deformed shape in the photograph of Figure 13(b).
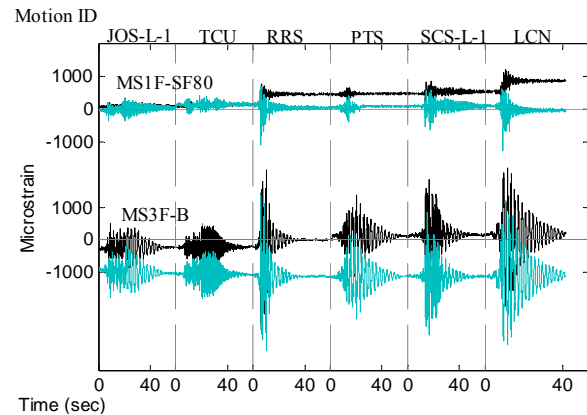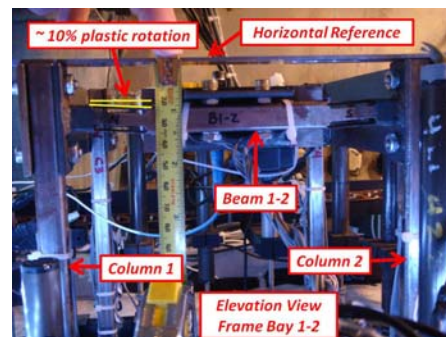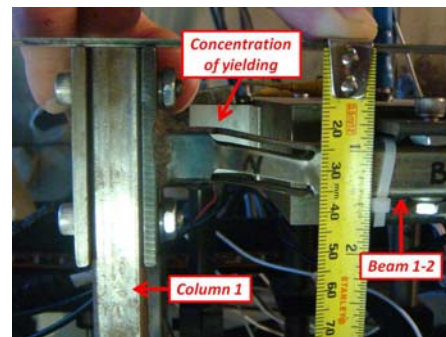

Fig. 12. Strain time-histories for the northwestern-most fuse of the 1st floor in both MS1F_SF80 and MS3F_B. Black is the top flanges of the respective hinges, while blue is the bottom.

(a) West frame bay spanning between columns 1 and 2

(b) Northwestern fuse

Fig. 13. Photographs to the damage to fuse members post-spin for model MS1F_SF80.

Strain measurements can be used to calculate average local curvature in the structural fuses. Structural damage can then be summarized in terms of the curvature ductility at each hinge location. Maximum curvature ductility demand $(\mu_\phi)_{max}$ is defined as the maximum curvature ϕ_{max} measured during each motion divided by the yield curvature ϕ_y of the hinge. The yield curvature can be estimated from material test data or bending calibration tests. Figure 14 plots the curvature-histories of the northwestern-most hinge in the 1st floor of MS3F_B. This data shows that initial structural yielding occurred during the 9th motion, while additional accumulation of plastic rotation occurred during the 10th and 17th motions. It is interesting to note that the 9th, 10th and 17th motion are all classified as near fault, higher intensity (NF-H1) motions, with peak input accelerations ranging from 0.24 to 0.57g's and peak input velocities ranging from 33 to 52 cm/sec (Mason et al., 2010). Yielding was not evident from visual inspection of model MS3F_B post Test-1, however strain and curvature data clearly indicates that plastic strain cumulated. Because shear failure was not observed in the hinges of MS3F_B, curvature is a reliable indicator of structural damage.
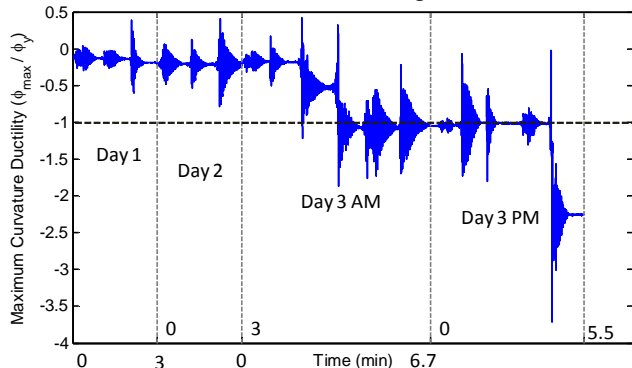

Fig. 14. *Curvature time history of the Northwestern-most fuse of the 1st floor of model MS3F_B. Time measurements are reference to total time of the motions applied during the various spin days.*

RESPONSE OF THE MODEL BUILDING-FOUNDATION SYSTEMS FOR ALL MOTIONS

Acceleration Demands

The case-study analysis of motion LCN included characterization of the acceleration amplification in the two building-foundation systems. In this section, we investigate acceleration amplification for all input motions. The soil-surface FFM motion is treated as the sole input to the systems (for the basement foundation, this is not entirely true since the basement bottom-level FFM is quite different from the surface FFM; Figure 10 (a) displays this phenomenon). Adopting the motion categorization developed by Mason et al. (2010), the symbols shown in Figures 15 and 16 reflect bins related to motions of NF, LI = near fault lower intensity; NF, HI = near fault higher intensity; Ord, LI = ordinary lower intensity; and Ord, HI = ordinary higher intensity.

In Figure 15, the peak roof accelerations (PRAs) are plotted against the peak ground accelerations (PGAs). First, one can

see that the motions roughly form clusters in accordance with their categorization. Second, the two models differ in that MS1F_SF80 tends to amplify all motions (14 out of 16 motions are amplified relative to the PRA's); however, model MS3F_B tends to be less effective in amplifying the input motions – 5 out of 16 motions are not amplified.
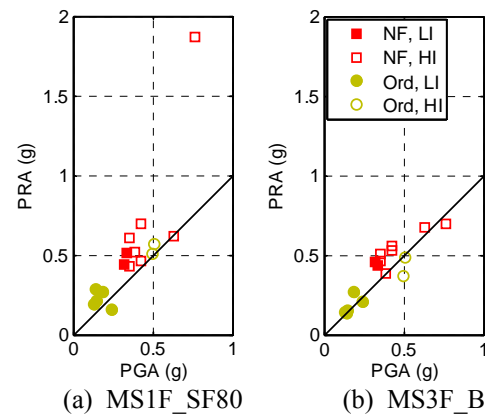

Fig. 15 *Peak roof acceleration (PRA) versus peak ground acceleration (PGA).*

To further investigate the effects on the models of the different input motions, un-correlated acceleration amplification factors are calculated at the floor levels for both models. In Figure 16, the distribution with normalized height of the un-correlated acceleration amplification factor, defined as $\Omega = PFA_n / PGA$, where PFA_n = peak floor acceleration of the nth floor, are shown presented. Comparing the Ω values for the two models, MS1F_SF80 results in larger values and dispersion than model MS3F_B. The largest Ω factor is about 2.6, which is due to motion PRI, classified as a NF-HI motion. Second, by linearly connecting the average amplification factors within each category, the near fault motions systematically cause the largest acceleration amplification (red solid and dashed lines). It is also interesting to note that from the profiles in Figure 16(b), model MS3F_B demonstrates a strong 2nd mode behavior. This is consistent with the observations noted in the case history analysis of motion LCN (Figure 10).
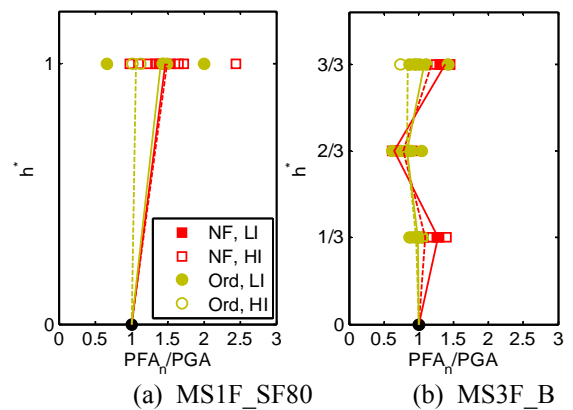

Fig. 16. *Uncorrelated acceleration amplification factors at floor levels for both model structures subject to all motions.*

CONCLUSIONS

The behavior of two model building-foundation systems is investigated during progressive earthquake shaking imposed in a 55-g centrifuge environment. Nonlinear behavior of the models is achieved either through nonlinear soil-foundation compliance or more readily through designed inelastic fuses strategically placed in the superstructure of the models. Earthquake shaking caused yielding of both models, which was evident in the measured strain time histories and post-spin physical inspections. Amplification of demands to the superstructure is evaluated using measured accelerations. For the taller model, higher mode effects are observed to significantly contribute to the systems response. In these tests, the models are placed in isolation, hence provide a baseline comparison to subsequent testing where structure-soil-structure-interaction will be studied. The importance of this 'city block' issue has yet to observe needed recognition in design practice. The reader is encouraged to track the progress of this project at the project website: http://www.nees-cityblock.org/.

ACKNOWLEDGMENTS

REFERENCES

Applied Technology Council (ATC). [2007], "Guidelines for seismic performance assessment of buildings", Report ATC-58, Redwood City, CA (*www.atcouncil.org*).

American Society of Civil Engineers (ASCE) [2007]. "Seismic Rehabilitation of Existing Buildings", ASCE/SEI 41-06, 2007, Reston, Virginia.

Bielak, J. [1975]. "Dynamic behaviour of structures with embedded foundations", Earthquake Engineering And Structural Dynamics, 3:259–274.

Bielak, J., Askan A., Fernandez A., Fenves, G.L., Stojadinovic, B., Park, J., Petropoulos, G. Haupt, T., King, R. and Meyer, J. [2005]. "Simulation for determining the seismic performance of urban regions", *Proceedings of Sixth European Conference on Structural Dynamics*, Paris, France.

Boulanger, R. W. [2000]. "The pysimple1, qzsimple1 and tzsimple1 material documentation", Documentation for the OpenSees platform available at: http://opensees.berkeley.edu/.

Cremer, C., Pecker, A. and Davenne, L. (2001). "Cyclic macro-element of soil structure interaction: Material and geometrical nonlinearities." *Int. Journal of Num. Anal. Meth. Geomech.*, Vol. 25, 1257-1284

Ganuza, E.A. B. [2006]. "Seismic Behavior of Hybrid Lateral-Force-Resisting Systems", Master Thesis, Department of Civil, Structural and Environmental Engineering, the State University of New York at Buffalo.

FEMA. [2000]. "Pre-standard and commentary for the seismic rehabilitation of buildings", Technical Report-356, Federal Emergency Management Agency.

FEMA. [2005]. "Improvement of nonlinear static seismic analysis procedures", Technical Report-440, Federal Emergency Management Agency.

Gajan. S. and Kutter, B.L. [2009]. "Contact Interface Model for Shallow Foundations Subjected to Combined Cyclic Loading", *Journal of Geotechnical and Geoenvironmental Engineering*, 135(3): 407-419.

Gerolymos, N. and Gazetas, G. [2006]. "Development of winkler model for static and dynamic response of caisson foundations with soil and interface nonlinearities", Soil Dynamics and Earthquake Engineering, 26(5):363 – 376.

Ghergu, M. and Ionescu, I.R. [2009]. "Structure-soil-structure coupling in seismic excitation and 'City Effect'", International Journal of Engineering Science, 47:342–354.

Grobya, J. and Wirgin, A. [2008], "Seismic motion in urban sites consisting of blocks in welded contact with a soft layer overlying a hard half-space", Geophysical Journal nternational , Vol. 172, pp. 725–758.

Harden, C., Hutchinson, T. C. and Moore, M. [2006]. "Investigation into the Effects of Foundation Uplift on Simplified Seismic Design Procedures," Earthquake Spectra, Vol. 22(3), pp. 663-692.

Housner, G. W. [1963]. "The Behavior of Inverted Pendulum Structures During Earthquakes," Bull. Seism. Soc. Am., 53, 403-417.

James, G. H., Carne, T. G., Lauffer, J. P., and Nord, A. R. [1992]. ''Modal testing using natural excitation.'' *Proc., 10th Int. Modal Analysis Conf.*, San Diego.

Kham, M. and Semblat, J. [2006], "Seismic site-city interaction: main governing phenomena through simplified numerical models", Bulletin of the Seismological Society of America , Vol. 96, pp. 1934–1951.

Lee, T. and Wesley, D. [1973], "Soil-structure interaction of nuclear reactor structures considering through-soil coupling between adjacent structures", Nuclear Engineering and Design, Vol. 24, pp. 374 – 387.

Luco, J. [1969], "Dynamic interaction of a shear wall with the soil", J. Eng. Mech. Div., Vol. 95, pp. 333–346

Luco, J. and Contesse, L. [1973], "Dynamic structure-soil-structure interaction", Bulletin of the Seismological Society of America , Vol. 63, pp. 1289–1303.

Martin, G. and Lam, I. P. [2000], "Earthquake Resistant Design of Foundations-retrofit of Existing Foundations," Proceedings of GeoEngineering 2000 Conference, Melbourne, Australia.

Mason, H.B., Bray, J.D, Jones, K.C, Chen, Z., Hutchinson, T.C., Trombetta, N.W., Choy, B.Y, Kutter, B.L., Fiegel, G.L., Montgomery, J., Patel, R.J., Reitherman, R.D., Bolisetti, C. and Whittaker, A.S. [2010]. "Earthquake Input Motions and Seismic Site Response in Centrifuge Tests Examining SFSI Effects", Proceedings of Fifth International Conference on Recent Advances in Geotechnical Earthquake Engineering and Soil Dynamics, San Diego, USA. (In Review).

Mazzoni, S., F. McKenna, M. H. Scott, and G. L. Fenves [2009]. Open System for Engineering Simulation User-Command-Language Manual, version 2.0, Pacific Earthquake Engineering Research Center, University of California, Berkeley. <http://opensees.berkeley.edu/>.

Mylonakis, G. and Gazetas, G. [2000] "Seismic soil-structure interaction: beneficial or detrimental?" Journal of Earthquake Engineering , Vol. 4, No. 3 pp. 277-301.

Pecker, A. and Pender, M. [2000], "Earthquake Resistant Design of Foundations: New Construction," Proceedings, GeoEngineering 2000 Conference, Melbourne, Australia.

Pitilakis, K., Kirtas, E., Sextos, A., Bolton, M., Madabhushi, G. and Brennan, A. [2004], "Validation by Centrifuge Testing of Numerical Simulations for Soil-foundation-structure Systems," Proceedings 13th World Conf. Earthquake Engineering, Vancouver, Canada.

Raychowdhury, P. and Hutchinson, T.C. [2009]."Performance evaluation of a nonlinear Winkler-based shallow foundation model using centrifuge test results", Earthquake Engineering and Structural Dynamics , Vol. 38, pp. 679–698.

Stewart, J., Seed, R. and Fenves, G. F. [1999a], "Seismic soil-structure interaction in buildings ii: Empirical findings",
Journal of Geotechnical and Geoenvironmental Engineering, Vol. 26, pp. 38–48.

Trifunac, M. [1972], "Interaction of a shear wall with the soil for incident plane SH waves", Bulletin of the Seismological Society of America, Vol. 62, pp. 63–83.

Veletsos, A. and Meek, J. [1974], "Dynamic behavior of building-foundation systems", Earthquake Engineering & Structural Dynamics , Vol. 3, pp. 121–138.

Wong, H. and Trifunac, M. [1975], "Two-dimensional, antiplane, building-soil-building interaction for two or more buildings and for incident planet SH waves", Bulletin of the Seismological Society of America , Vol. 65, pp. 1863–1885.